E1-2019-31

A. A. Terekhin *, Yu. V. Gurchin, A. Yu. Isupov, A. N. Khrenov, A. K. Kurilkin, P. K. Kurilkin, V. P. Ladygin, N. B. Ladygina, S. M. Piyadin, S. G. Reznikov, M. Janek [1]

THE DIFFERENTIAL CROSS SECTION IN DEUTERON–PROTON ELASTIC SCATTERING AT 500, 750 AND 900 MeV/NUCLEON

Submitted to "European Physical Journal A"

* E-mail: aterekhin@jinr.ru

[1] Faculty of Electrical Engineering and Information Technology, University of Zilina, Zilina, Slovakia

Терехин А. А. и др. E1-2019-31
Дифференциальное сечение дейтрон-протонного упругого рассеяния при 500, 750 и 900 МэВ/нуклон

Представлены результаты по дифференциальному сечению dp-упругого рассеяния, полученные на станции внутренних мишеней нуклотрона при энергии 500, 750 и 900 МэВ/нуклон. Данные получены в угловом диапазоне 70–120° в с. ц. м. Угловые зависимости сравнивались с мировыми данными при близких энергиях, а также с теоретическими вычислениями, выполненными в рамках релятивистской теории многократного рассеяния. Поведение дифференциального сечения при фиксированных углах рассеяния в диапазоне полной энергии $\sqrt{s} = 3{,}1-3{,}42$ ГэВ находится в разумном согласии с предсказаниями правил кваркового счета.

Работа выполнена в Лаборатории физики высоких энергий им. В. И. Векслера и А. М. Балдина ОИЯИ.

Препринт Объединенного института ядерных исследований. Дубна, 2019

Terekhin A. A. et al. E1-2019-31
The Differential Cross Section in Deuteron–Proton Elastic Scattering at 500, 750 and 900 MeV/Nucleon

The results on the differential cross section of dp elastic scattering obtained at the Internal Target Station at the Nuclotron of JINR at energies of 500, 750 and 900 MeV/nucleon are presented. The measurements have been performed using an unpolarized deuteron beam and a polyethylene foil target. The data have been obtained in the angular range of 70°–120° in the cms. The angular dependences of the data from the present experiment are compared with the world experimental data obtained at similar energies as well as with the theoretical calculations performed within the relativistic multiple scattering theory. The behavior of the differential cross section at the fixed scattering angles covering the total cms energy region of $\sqrt{s} = 3.1-3.42$ GeV is in qualitative agreement with the s-power-law dependence.

The investigation has been performed at the Veksler and Baldin Laboratory of High Energy Physics, JINR.

Preprint of the Joint Institute for Nuclear Research. Dubna, 2019

INTRODUCTION

Elastic nucleon–deuteron scattering is the simplest process of the hadron nucleus collisions which is used to understand the structure of nucleon–nucleon and three-nucleon interactions. The study of dp elastic scattering at high energies is aimed to obtain the information on the role of relativistic effects, contribution of baryonic resonances exchanges and manifestation of the fundamental degrees of freedom of the strong interaction.

Since the first nucleon–deuteron experiments performed as early as the 1950s [1–5], a significant amount of data at energies above 400 MeV/nucleon has been accumulated both on the differential cross section and on polarization observables [6–17]. Recently new results on the cross section and deuteron analyzing powers [18–20] have been obtained at the Internal Target Station (ITS) [21, 22] at the Nuclotron.

The forward-angle dp elastic scattering at high energies is successfully described by the Glauber–Sitenko diffraction multiple-scattering theory [23, 24]. The interference between the single- and double-scattering amplitudes [25] including the D-state in the deuteron wave function (DWF) allowed one to explain the filling of the cross section diffractive minimum [26]. Further the multiple scattering formalism for deuteron–proton elastic scattering up to 1 GeV/nucleon has been developed as an extension of the Glauber–Sitenko theory incorporating the complete spin structure and the corrections to the eikonal approximation [27]. The consideration of the relativistic and off-energy-shell effects playing an important role at the scattering angles larger than 30° in the cms [28, 29] allowed describing satisfactorily the angular behavior of the dp elastic scattering cross section up to 600 MeV/nucleon using CD-Bonn DWF [30] and the SP07 solution of the phase-shift analysis for elastic nucleon–nucleon scattering [31].

The differential cross section of dp elastic scattering at backward angles in the cms demonstrates a strong energy dependence and an enhancement in the vicinity of the Δ-isobar excitation. In the model of Kerman and Kisslinger [32] such behavior is interpreted as due to the admixture of NN^*-state in the standard deuteron wave function. It is shown that the interference of the Δ-isobar excitation with

the pole mechanism could provide a satisfactory description of the energy dependence of the dp elastic scattering cross section at backward angles [33, 34]. The description of the cross section data improves significantly when the contribution from the three-baryon resonances obtained in the bag model as the nine-quark states with hidden color is added [35]. However, the double scattering with a nucleon in the intermediate state has not been considered. The cross section and polarization observables in dp elastic backward scattering were studied within a covariant approach based on the Bethe–Salpeter equation [36]. It was shown that the relativistic effects become significant already at proton momenta in the deuteron rest frame of 0.4–0.5 GeV/c. The one-pion exchange contribution is essential to describe the cross section data [37]. A good description of the differential cross section of the dp elastic scattering in a whole angular range at the deuteron energies between 500 and 1300 MeV was obtained within the multiple scattering expansion formalism taking into account one-nucleon exchange, single and double scattering and Δ-isobar excitation [38]. The contribution of the Δ-isobar mechanism is essential at backward angles growing with the initial deuteron energy.

According to the constituent counting rules (CCR) [39–41], the scaling behavior of the differential cross section of binary reactions can be an indication of the transition from hadrons to quark–gluon degrees of freedom. A self-similarity [39], perturbative QCD [40] and AdS/QCD correspondence [41] approaches predict s^{-16} scaling behavior for the dp elastic scattering cross section at the fixed angles in the cms. In this respect, new data on dp elastic scattering obtained at large transverse momenta could shed light on the manifestation of the fundamental degrees of freedom in nuclear interactions.

This paper presents new experimental data on the angular dependence of the dp elastic scattering differential cross section at the beam kinetic energies of 500, 750 and 900 MeV/nucleon obtained at ITS at the Nuclotron [21]. The angular range of the measurements corresponds to large transverse momenta of the scattered deuteron (up to $\sim$900 MeV/c). The paper is organized as follows. Section 1 describes the details of the experiment and data analysis. The procedure of the differential cross section evaluation is given in Section 2. The comparison of the obtained results with the theoretical predictions within the relativistic multiple-scattering model and CCR is presented in Section 3. The conclusions are drawn in the last section.

1. EXPERIMENT AND DATA ANALYSIS

The measurements were performed using ITS [21] at the Nuclotron with a control and data acquisition system [22]. The ITS consists of a spherical scattering chamber and a target sweeping system. The scattering chamber is fixed on the

flanges of the Nuclotron ion tube. The disk mounting six different targets is located on the axle of the stepper motor. A target used for the measurement is moved to the center of the ion tube when the particles are accelerated up to the required energy. A 10 μm polyethylene (CH_2) foil was used as a proton target. A 8 μm carbon (^{12}C) wire was used to evaluate the background originating from the carbon content in CH_2. The effect on the hydrogen was obtained using $CH_2 - C$ subtraction. A signal from the target position monitor [42] was used to tune the accelerator parameters to bring the interaction point close to the center of the ITS chamber.

A detector support mounting 6 plastic scintillation counters was placed downstream the ITS spherical chamber. Each plastic scintillation counter was coupled to a Hamamatsu H7416MOD photo-multiplier tube. Two pairs of scintillation detectors were used to register scattered deuterons and recoil protons from dp elastic scattering in kinematical coincidence over the cms angular range of $\sim$75°–120°. Two proton detectors were installed on the left and on the right at a distance of 580 mm from the target. The angular span of one proton detector was 2° in the laboratory frame, which corresponds to $\sim$4° in the cms. Two deuteron detectors were placed at the scattering angles of deuterons coinciding kinematically with the protons or left and right scattering. A pair of the scintillation detectors was placed to register two protons from quasi-elastic pp scattering at $\theta_{pp} = 90°$ in the cms in the horizontal plane to monitor the beam luminosity. These detectors remained stationary during data taking at the fixed energy of the beam. The deuteron and quasi-elastic pp detectors were placed at a distance of 560 mm from the target in front of the proton detectors. The details of the detection system description can be found in [20].

The data on the angular dependences of dp elastic scattering were obtained at energies of 500, 750 and 900 MeV/nucleon. The additional measurements at 650 and 700 MeV/nucleon at several scattering angles were performed to evaluate the normalization coefficients.

Selection of dp elastic scattering events was based on the kinematical coincidence of scattered deuterons and recoil protons by the scintillation counters at several angles in the cms. The energy loss correlation and time-of-flight difference for the signals from each proton–deuteron detector pair were used. The correlation of the deuteron and proton energy losses at 500 MeV/nucleon and $\theta_{\rm cm} \sim 76°$ for the CH_2 target is shown in Fig. 1. Wide graphical cut shown by the dashed curve in Fig. 1 was imposed to minimize the losses of dp elastic scattering events.

The time difference between the signals from the deuteron and proton detectors gated by the correlation on the energy losses at 500 MeV/nucleon and $\theta_{\rm cm} \sim 76°$ for the CH_2 target is shown in Fig. 2. The effects on proton and carbon content of CH_2 are clearly seen. The contribution from carbon increases with increasing beam energy. The time distribution is the sum of useful events

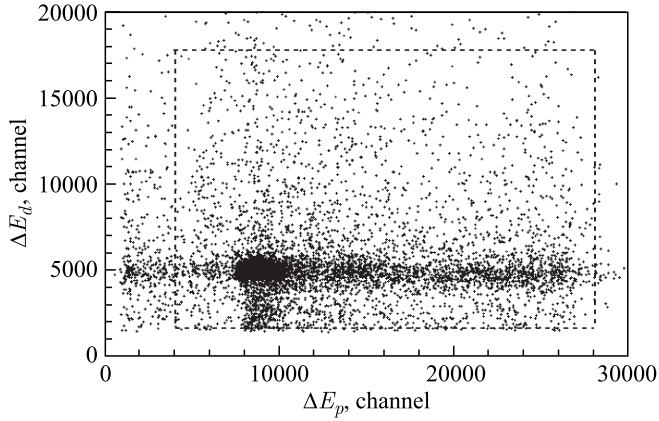

Fig. 1. Correlation of the deuteron and proton energy losses at 500 MeV/nucleon and scattering angle $\theta_{\rm cm} \sim 76^\circ$ for the CH_2 target. The dashed line represents the graphical cut for the dp elastic scattering events selection

and the background from random coincidences. The number of the background events contained in region I in Fig. 2 was estimated as a sum of the events in regions II and III. The width of intervals II and III was taken to be such that their sum was equal to the width of region I. The amplitude spectrum for the proton detector was obtained as a difference of the amplitude spectra with the cut on time difference in the vicinity of the H_2 signal (region I) and with the cut in regions II and III [20].

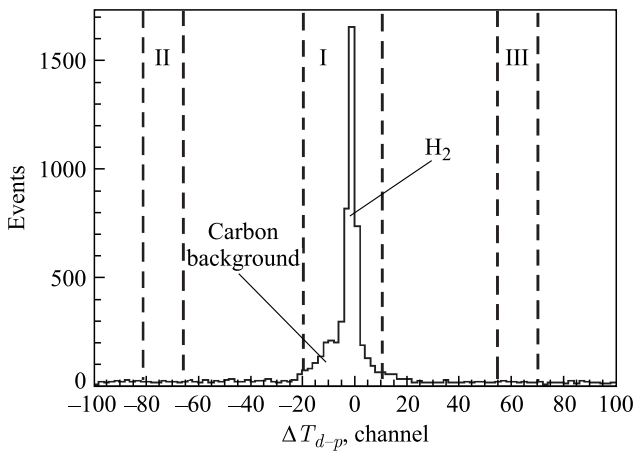

Fig. 2. The time difference between the signals from the deuteron and proton counters at 500 MeV/nucleon and $\theta_{\rm cm} \sim 76^\circ$ for the CH_2 target. The vertical lines indicate the boundaries of the dp elastic scattering events selection (region I) and of the random coincidences background (regions II and III)

The final selection of dp elastic events was performed by the $CH_2 - C$ subtraction of the amplitude spectra of proton detectors. Figure 3 demonstrates the $CH_2 - C$ subtraction procedure for the data obtained at 500 MeV/nucleon and $\theta_{cm} \sim 76^\circ$. The CH_2- and normalized C-amplitude distributions are given in Fig. 3, *a* by the open and filled histograms, respectively. The vertical solid lines delimit the interval for the evaluation of the normalization coefficient for the subtraction of the carbon background k, which is determined in the interval of $a_{min} < a < a_{max}$, where a are channels of amplitude distributions obtained on the CH_2 and C targets:

$$k = \frac{N_{CH_2}|_{a_{min}<a<a_{max}}}{N_C|_{a_{min}<a<a_{max}}}. \quad (1)$$

Here, N_{CH_2} and N_C are the CH_2- and C-integrals over the a interval delimited by the solid vertical lines in Fig. 3, *a*. The number of dp elastic scattering events N_{dp} and its statistical error ΔN_{dp} can be determined as

$$\begin{aligned} N_{dp} &= N_{CH_2} - kN_C, \\ \Delta N_{dp} &= \sqrt{N_{CH_2} + k^2 N_C}, \end{aligned} \quad (2)$$

where N_{CH_2} and kN_C are the integrals of the total CH_2 and normalized C spectra. The region of dp elastic scattering events is bounded in Fig. 3, *b* by the vertical dashed lines.

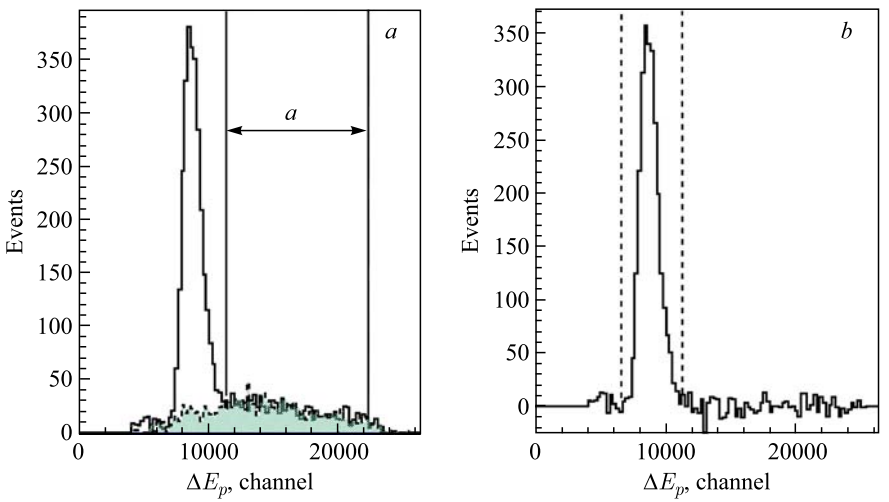

Fig. 3. $CH_2 - C$ subtraction for $\theta_{cm} \sim 76^\circ$ at an energy of 500 MeV/nucleon: *a*) the CH_2- and normalized C-distributions given by the open and filled histograms, respectively, the vertical solid lines show the interval of the normalization; *b*) the result of $CH_2 - C$ subtraction, the vertical dashed lines delimit the domain of dp elastic scattering events

2. DIFFERENTIAL CROSS SECTION EVALUATION

The expression for the differential cross section in the cms has the following form:

$$\left(\frac{d\sigma}{d\Omega}\right)_{\rm cms} = \frac{N_{dp}}{d\Omega^D_{\rm lab}} \frac{k_{pp}}{N_{\rm CH_2}} J_D C_{\rm norm}. \quad (3)$$

Here N_{dp} is the number of dp elastic scattering events, $d\Omega^D_{\rm lab}$ is the effective solid angle of the deuteron detector in the laboratory frame under the conditions of its kinematical coincidence with the proton counter, $N_{\rm CH_2}$ is the number of reconstructed pp quasi-elastic scattering events at $\theta_{pp} = 90^\circ$ in the cms obtained on the polyethylene target, k_{pp} is the correction factor for the background coming from the carbon in the $N_{\rm CH_2}$ value, J_D is the Jacobian transformation for the transition from the laboratory to the cms, and $C_{\rm norm}$ is the normalization coefficient for the given deuteron energy.

The effective solid angle $d\Omega^D_{\rm lab}$ and Jacobian transformation J_D were calculated using the Pluto event generator [43] as

$$d\Omega^D_{\rm lab} = \left(S^D_{\rm eff}\right)_{\rm lab}/r^2, \;\; J_D = d\Omega^D_{\rm lab}/d\Omega^D_{\rm cm}, \quad (4)$$

where $\left(S^D_{\rm eff}\right)_{\rm lab}$ is the effective deuteron detector area, r is the distance from the detector to the target, $d\Omega^D_{\rm cm}$ is the effective solid angle of the deuteron detector in the cms.

The coefficient k_{pp} was calculated as the ratio of the total number of pp quasi-elastic events obtained on the CH_2 target without carbon background subtraction to the number of events after subtraction for all dp elastic scattering angular settings. The k_{pp} values for different energies are given in Table 1. One can see that k_{pp} grows with increasing energy.

Table 1. The carbon background correction factor k_{pp} for pp quasi-elastic scattering events on the polyethylene target for different deuteron energies

Energy, MeV/nucleon	k_{pp}	$\Delta(k_{pp})_{\rm stat}$	$\Delta(k_{pp})_{\rm sys}$
500	1.33	0.0014	0.003
750	1.70	0.005	0.004
900	1.89	0.006	0.009

The normalization coefficients $C_{\rm norm}$ at 500 and 900 MeV/nucleon were calculated using the data obtained at 700 MeV/nucleon. The measurements at this energy were performed for the scattering angle $\theta_{\rm cm}$ = 75.8°. The obtained result for the differential cross section was normalized to the data taken at the same angle $\theta_{\rm cm}$ [19]. The differential cross section value of (0.031 ± 0.004) mb/sr (the error is the total) was calculated as the result of a linear spline function

between the data obtained at $\theta_{\rm cm} = 72.3^\circ$ and $\theta_{\rm cm} = 77.5^\circ$. The normalization coefficient was found to be $C^{700}_{\rm norm} = (6.7 \cdot 10^{-3} \pm 9.0 \cdot 10^{-4})$ mb. The error is due to the error of the data obtained earlier at 700 MeV/nucleon [19].

The normalization coefficients $C^{500(900)}_{\rm norm}$ at energies of 500 and 900 MeV/nucleon were taken as $C^{700}_{\rm norm}/R$, where R is the ratio of the differential cross sections for pp elastic scattering at energies of 700 and 500 (900) MeV/nucleon within the acceptance of the monitor scintillation detector:

$$R = \frac{\int \left(\frac{d\sigma}{d\Omega_{\rm cm}}\right)^{700} d\cos\theta_{\rm cm}}{\int \left(\frac{d\sigma}{d\Omega_{\rm cm}}\right)^{500(900)} d\cos\theta_{\rm cm}}. \quad (5)$$

Here the integration is performed within the angular acceptance of the monitor detector at 700 and 500(900) MeV/nucleon, respectively. The angular dependence of the pp elastic scattering cross section data was taken from Ref. [44].

The normalization coefficient $C^{650}_{\rm norm}$ at an energy of 650 MeV/nucleon was obtained for calculation of the differential cross section at 750 MeV/nucleon. The world data at 641 MeV/nucleon [10] were approximated by a function taken in the form $f(\theta_{\rm cm}) = P_0 \cdot e^{P_1\theta_{\rm cm}}$ in the angular range of $71^\circ < \theta_{\rm cm} < 90^\circ$. In this range, the data at 650 MeV/nucleon obtained in our experiment were approximated by a function $F(\theta_{\rm cm}) = C \cdot e^{P_1\theta_{\rm cm}}$ with a fixed parameter P_1. The normalization coefficient calculated as $C^{650}_{\rm norm} = P_0/C$ equals $(5.6 \cdot 10^{-2} \pm 1.3 \cdot 10^{-2})$ mb. The error of the $C^{650}_{\rm norm}$ coefficient was determined by the statistical errors of the data obtained in our experiment and uncertainty of the P_0 parameter. The normalization coefficient at an energy of 750 MeV/nucleon was calculated as $C^{750}_{\rm norm} = C^{650}_{\rm norm}/R$, where R is the ratio of the pp elastic scattering cross sections at 650 and 750 MeV/nucleon within the monitor scintillation detector acceptance.

The values of the R and $C^{500,750,900}_{\rm norm}$ coefficients are given in Table 2.

Table 2. The values of the R and $C^{500,750,900}_{\rm norm}$ coefficients

Energy, MeV/nucleon	R	$C_{\rm norm}$, mb
500	0.50 ± 0.01	$1.4 \cdot 10^{-2} \pm 2.6 \cdot 10^{-3}$
750	1.66 ± 0.03	$3.4 \cdot 10^{-2} \pm 7.9 \cdot 10^{-3}$
900	2.31 ± 0.03	$2.9 \cdot 10^{-3} \pm 3.9 \cdot 10^{-4}$

The statistical error of the differential cross section was determined by the statistical error of dp elastic scattering events ΔN_{dp} calculated according to Eq. (2), the statistical error of the number of reconstructed pp quasi-elastic scattering events $\sqrt{N_{\rm CH_2}}$ and the statistical error of the carbon background correction factor $\Delta\left(k_{pp}\right)_{\rm stat}$ (see Table 1).

Several systematic errors for each data point were taken into account. The normalization coefficient error $\Delta C_{\rm norm}$ was general for all data points obtained at a given energy. The $\Delta\left(k_{pp}\right)_{\rm sys}$ and $\Delta N_{dp}^{\rm sys} = \Delta k \cdot N_{\rm C}$ were the uncertainties of the carbon background subtraction procedure for the luminosity monitor and useful events, respectively. The errors of the solid angle of the deuteron detector $\Delta d\Omega_{\rm lab}^{D}$ and the Jacobian transformation ΔJ_D were estimated using a Monte Carlo simulation with Pluto generator [43]. A typical total systematic error is about 30%.

The differential cross section data obtained at energies of 500, 750 and 900 MeV/nucleon are given in Tables 3, 4 and 5, respectively.

Table 3. Differential cross section of dp elastic scattering at 500 MeV/nucleon

$\theta_{\rm cm}$, deg.	$d\sigma/d\Omega_{\rm cm}$, μb/sr	$\Delta\left(d\sigma/d\Omega_{\rm cm}\right)_{\rm stat}$, μb/sr	$\Delta\left(d\sigma/d\Omega_{\rm cm}\right)_{\rm sys}$, μb/sr
75.9	61.54	1.28	23.4
81.3	57.70	0.83	21.1
106.5	34.56	0.94	15.1
112.5	35.62	0.65	15.4
116.7	33.45	0.58	15.1
119.7	34.19	0.94	12.8

Table 4. Differential cross section of dp elastic scattering at 750 MeV/nucleon

$\theta_{\rm cm}$, deg.	$d\sigma/d\Omega_{\rm cm}$, μb/sr	$\Delta\left(d\sigma/d\Omega_{\rm cm}\right)_{\rm stat}$, μb/sr	$\Delta\left(d\sigma/d\Omega_{\rm cm}\right)_{\rm sys}$, μb/sr
78.9	25.19	2.07	8.23
83.7	24.93	1.41	8.14
88.8	18.82	1.88	6.05
93.9	18.03	2.10	5.55
98.7	14.51	2.08	4.88

Table 5. Differential cross section of dp elastic scattering at 900 MeV/nucleon

$\theta_{\rm cm}$, deg.	$d\sigma/d\Omega_{\rm cm}$, μb/sr	$\Delta\left(d\sigma/d\Omega_{\rm cm}\right)_{\rm stat}$, μb/sr	$\Delta\left(d\sigma/d\Omega_{\rm cm}\right)_{\rm sys}$, μb/sr
75.9	17.97	1.17	5.41
86.3	10.00	0.93	3.28
96.4	5.21	0.93	1.70
101.6	3.45	0.48	1.11
104.2	4.33	0.70	1.74
111.4	3.14	0.74	1.23

3. RESULTS AND DISCUSSION

The differential cross section data obtained in the present experiment at energies of 500, 750 and 900 MeV/nucleon are shown by the solid squares in Figs. 4, 5 and 6, respectively. Only statistical errors are given. One can see reasonable agreement of the Nuclotron data with the results from the previous experiments [6, 10, 12] represented by the open symbols.

The theoretical curves in Figs. 4–6 correspond to the predictions of the relativistic multiple scattering model [28, 29, 38]. In this approach, the expression for the reaction amplitude was obtained by iterating AGS equations for dp elastic scattering up to second-order terms of two-particle t-matrices. As a result, four contributions were included in consideration: one-nucleon exchange (ONE), single-scattering (SS), double-scattering (DS) terms, and term with Δ-isobar excitation in the intermediate state. These terms are presented schematically in Fig. 7.

The curves in Figs. 4–6 correspond to the calculation results taking into account different reaction mechanisms. The predictions taking into consideration only ONE and single nucleon–nucleon scattering are presented by the dotted lines. The dashed curves correspond to the calculations considering not only ONE+SS but also double nucleon–nucleon scattering. The results presented by the full lines include in consideration ONE+SS+DS and also Δ-isobar in the intermediate state.

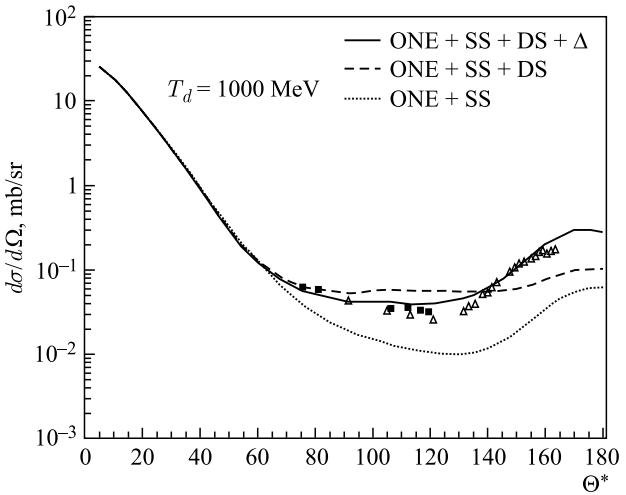

Fig. 4. Differential cross section of dp elastic scattering at ∼500 MeV/nucleon. The solid squares and open triangles correspond to the data obtained in the present experiment at 500 and 470 MeV/nucleon [6], respectively. The curves are the predictions obtained within the relativistic multiple-scattering model [38] taking into account different reaction mechanisms

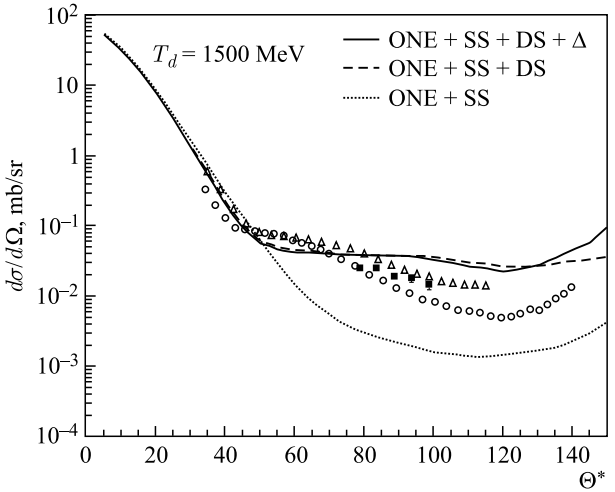

Fig. 5. Differential cross section of dp elastic scattering at ∼750 MeV/nucleon. The solid squares, open triangles and open circles are the data obtained in the present experiment at 750, 641 and 800 MeV/nucleon [10], respectively. The curves are the same as in Fig. 4

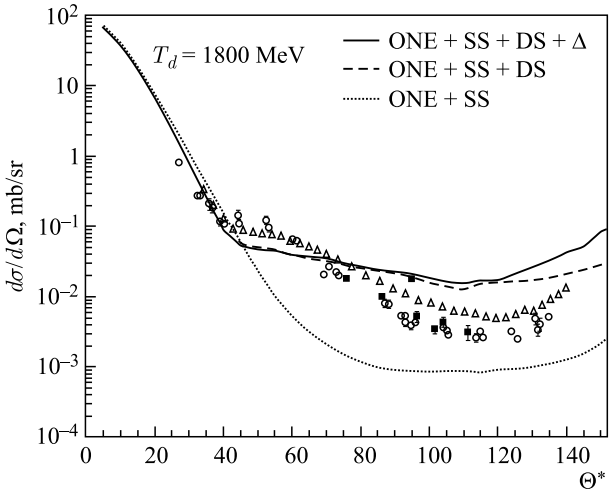

Fig. 6. Differential cross section of dp elastic scattering at ∼900 MeV/nucleon. The solid squares, open triangles and open circles are the data obtained in the present experiment at 750, 800 [10] and 1000 MeV/nucleon [12], respectively. The curves are the same as in Fig. 4

All these curves practically coincide at forward scattering angles. But the difference between the experimental data and the ONE+SS curves is significant at scattering angles above 60° and increases with growing energy. Additional

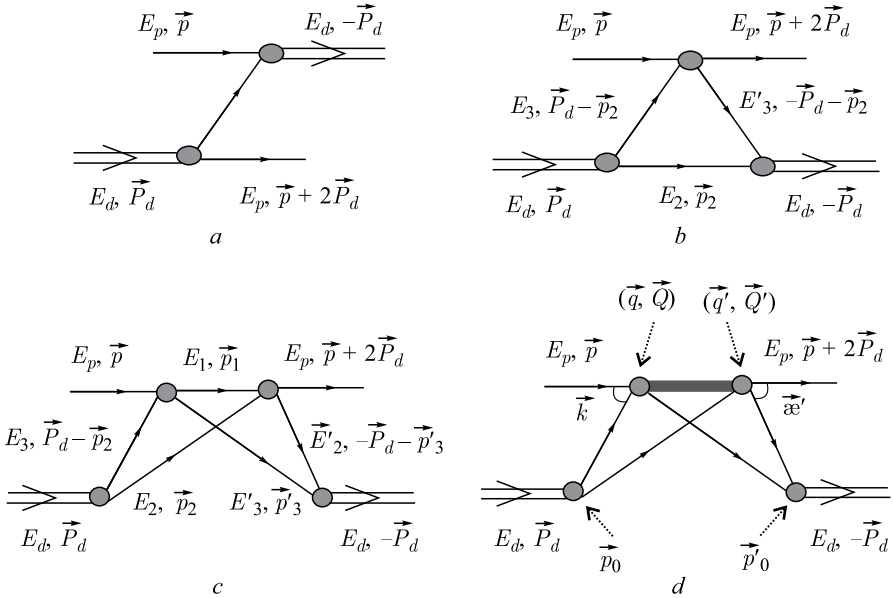

Fig. 7. The diagrams included in consideration: *a*) the one nucleon exchange diagram; *b*) the single scattering diagram; *c*) the double scattering diagram with a nucleon in the intermediate state; *d*) the double scattering diagram with Δ-isobar in the intermediate state

consideration of the DS-term improves the agreement between the data and theory in the angular range of 60°–140°. Influence of the Δ-isobar excitation is remarkable at backward scattering angles. Inclusion of the Δ-isobar term in consideration allows describing a rise of the differential cross sections at $\theta_{\rm cm} \geqslant 140°$ at an energy of 500 MeV/nucleon. As a result, good agreement between the data and theory is obtained in the whole angular range at 500 MeV/nucleon (Fig. 4). The description of the existing data at 750 MeV/nucleon is also quite reasonable (Fig. 5). But at higher energy the agreement between the data and theoretical predictions gets worse. We have a rather good description of the data at an energy of 900 MeV/nucleon only up to a scattering angle of about 90° (Fig. 6), but at larger angles the discrepancy between the data and theory is significant. Unfortunately, there is no data at backward angles at energies of 750 and 900 MeV/nucleon to estimate the quality of the theoretical predictions in this angular range.

In spite of the essential progress in the description of the differential cross section of dp elastic scattering, the angular region of 80°–130° remains the most problematic from the theoretical point of view. The considered reaction mechanisms are not enough to describe the experimental data in a whole angular range at energies above 500 MeV/nucleon. Moreover, the discrepancy between the data and theory at these scattering angles increases with growing energy.

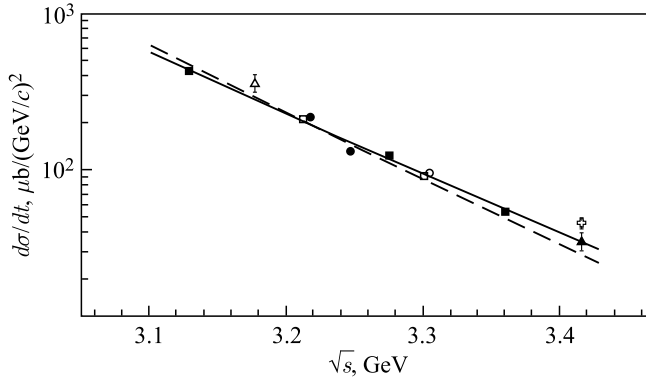

Fig. 8. Differential cross section of dp elastic scattering at $\theta_{\rm cm} \sim 82^\circ$. The solid squares are the data from the present experiment, solid triangles [19] and circles [20] are the data obtained earlier at the Nuclotron, open symbols are the results of the previous experiments [6–12]. The solid and dashed lines are the results of the fit by the functions $f \sim s^{-n}$ and $f \sim s^{-16}$, respectively

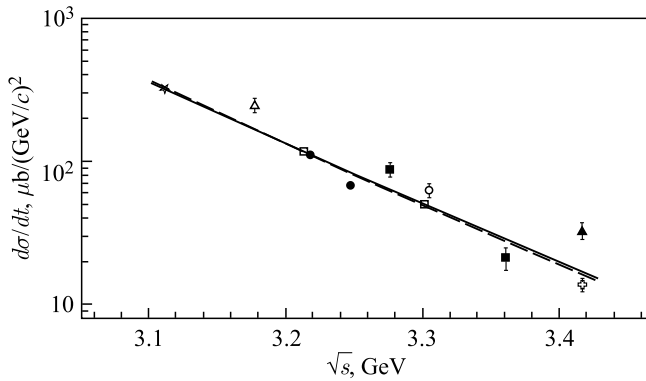

Fig. 9. Differential cross section of dp elastic scattering at $\theta_{\rm cm} \sim 95^\circ$. The symbols and lines are the same as in Fig. 8

Constituent counting rules predict s^{-16} scaling behavior for the dp elastic scattering cross section at the fixed angles in the cms at high energies and large transverse momenta [39–41]. The differential cross section of dp elastic scattering as a function of the total cms energy $\sqrt{s}$ is shown in Figs. 8, 9 and 10 for the cms scattering angles of $\sim$82°, $\sim$95°, and $\sim$111°, respectively. The solid squares, circles, and triangles are the results obtained at the Nuclotron in the present experiment, at 650 and 700 MeV/nucleon [20], and at 1000 MeV/nucleon [19], respectively. The world data [6–12] are shown by the open symbols. One can see a good consistency of the results from the Nuclotron and from the previous experiments.

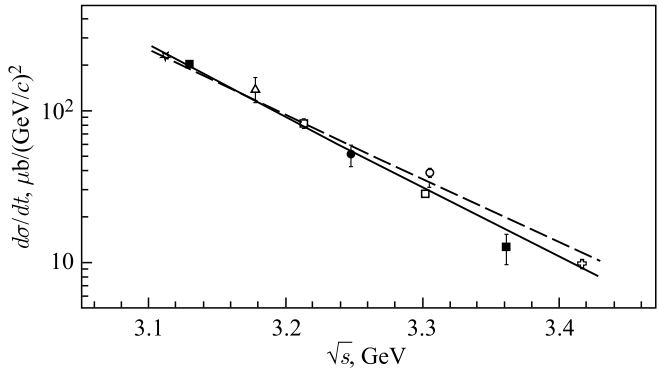

Fig. 10. Differential cross section of dp elastic scattering at $\theta_{\rm cm} \sim 111^\circ$. The symbols and lines are the same as in Fig. 8

The solid lines are the results of the experimental data parameterization by the function $f \sim s^{-n}$ over the range of $\sqrt{s} = 3.1{-}3.42$ GeV. The values of the n parameter obtained from the fit are 14.2 ± 0.2, 15.7 ± 0.2 and 17.4 ± 0.3 for $\theta_{\rm cm} \sim 82^\circ$, $\theta_{\rm cm} \sim 95^\circ$ and $\theta_{\rm cm} \sim 111^\circ$, respectively. The dashed lines are the s^{-16}-power-law dependences predicted by CCR [39–41]. One can see good agreement of the energy behavior of the experimental data at $\theta_{\rm cm} \sim 95^\circ$ with the CCR predictions, while the deviation from the s^{-16}-dependence is observed at scattering angles of $\sim 82^\circ$ and $\sim 111^\circ$ at $\sqrt{s} \geqslant 3.3$ GeV. On the other hand, the data used for the analysis were obtained in various experiments since the 1960s with quite large statistical and systematic errors, which could influence the fitting results. Therefore, new precise systematic measurements at energies higher than $\sqrt{s} \geqslant 3.3$ GeV and at different scattering angles are required to make a conclusion about the validity of CCR [39–41] in dp elastic scattering.

CONCLUSIONS

The results on the differential cross section of dp elastic scattering have been obtained at ITS [21] at the Nuclotron at energies of 500, 750 and 900 MeV/nucleon at large transverse momenta of up to ∼900 MeV/c. The results are in reasonable agreement with the data obtained earlier.

The data have been compared with the calculations of the relativistic multiple scattering theory. It has been shown that taking into account the double-scattering and Δ-isobars excitation in the intermediate state improves the description of the experimental results. The Δ-isobar contribution becomes sizable at angles of $\theta_{\rm cm} > 80^\circ$. The best agreement of the experimental data with the theory predictions is observed at 500 MeV/nucleon. However, the discrepancy increases with increasing energy.

The energy behavior of the dp elastic scattering differential cross section at the fixed scattering angles of $\theta_{\rm cm} \sim 82^\circ$ and 111° and at $\sqrt{s} = 3.1{-}3.42$ GeV is in qualitative agreement with the s-power-law dependence. However, further check of the CCR [39–41] validity requires new precise systematic measurements at $\sqrt{s} \geqslant 3.3$ GeV.

Acknowledgments. The authors thank the Nuclotron crew for providing good conditions of the experiment. The work has been supported in part by the RFBR under grants No. 16-02-00203a and No. 19-02-00079a, by the Ministry of Education, Science, Research, and Sport of the Slovak Republic (VEGA Grant No. 1/0113/18), by JINR–Slovak Republic scientific cooperation programs in 2016–2019.

REFERENCES

1. *Shamberger R. D.* // Phys. Rev. 1952. V. 85. P. 424.
2. *Chamberlain O., Stern M. O.* // Phys. Rev. 1954. V. 94. P. 666.
3. *Chamberlain O., Clark D. D.* // Phys. Rev. 1956. V. 102. P. 473.
4. *Crewe A. V. et al.* // Phys. Rev. 1959. V. 114. P. 1361.
5. *Marshall L. et al.* // Phys. Rev. 1954. V. 95. P. 1020.
6. *Alder J. C. et al.* // Phys. Rev. C. 1972. V. 6. P. 2010.
7. *Booth N. E. et al.* // Phys. Rev. D. 1971. V. 4. P. 1261.
8. *Vincent J. S. et al.* // Phys. Rev. Lett. 1970. V. 24. P. 236.
9. *Boschitz E. T. et al.* // Phys. Rev. C. 1972. V. 6. P. 457.
10. *Gülmez E. et al.* // Phys. Rev. C. 1991. V. 5. P. 2067.
11. *Winkelmann E. et al.* // Phys. Rev. C. 1980. V. 21. P. 2535.
12. *Bennet G. W. et al.* // Phys. Rev. Lett. 1967. V. 19. P. 387.
13. *Haji-Saeid M. et al.* // Phys. Rev. C. 1986. V. 36. P. 2010.
14. *Igo G. et al.* // Phys. Rev. C. 1988. V. 38. P. 2777.
15. *Arvieux J. et al.* // Phys. Rev. Lett. 1983. V. 50. P. 19; Nucl. Phys. A. 1984. V. 431. P. 613.
16. *Ghazikhanian V. et al.* // Phys. Rev. C. 1991. V. 43. P. 1532.
17. *Glagolev V. V. et al.* // Eur. Phys. J. A. 2012. V. 48. P. 182.
18. *Kurilkin P. K. et al.* // Phys. Lett. B. 2012. V. 715. P. 61.
19. *Terekhin A. A. et al.* // Phys. Part. Nucl. Lett. 2015. V. 12. P. 695.
20. *Terekhin A. A. et al.* // Phys. Atom. Nucl. 2017. V. 80. P. 1061.
21. *Malakhov A. I. et al.* // Nucl. Instrum. Meth. Phys. Res. A. 2000. V. 440. P. 320.
22. *Isupov A. Yu. et al.* // Nucl. Instrum. Meth. Phys. Res. A. 2013. V. 698. P. 127.
23. *Glauber R. J.* // Lect. Theor. Phys. 1959. V. 1. P. 315.
24. *Sitenko G.* // Sov. Phys. Uspekhi. 1959. V. 2. P. 195.

25. *Franco V.* // Phys. Rev. Lett. 1966. V. 16. P. 944;
Franco V., Coleman E. // Phys. Rev. Lett. 1966. V. 17. P. 827.
26. *Harrington D. R.* // Phys. Rev. Lett. 1968. V. 21. P. 1496.
27. *Alberi G., Bleszynski M., Jaroszewicz T.* // Ann. Phys. (N.Y.) 1982. V. 142. P. 299.
28. *Ladygina N. B.* // Phys. Atom. Nucl. 2008. V. 71. P. 2039.
29. *Ladygina N. B.* // Eur. Phys. J. A. 2009. V. 42. P. 91.
30. *Machleidt R.* // Phys. Rev. C. 2001. V. 63. P. 024001.
31. http://gwdac.phys.gwu.edu
32. *Kerman A. K., Kisslinger L. S.* // Phys. Rev. 1969. V. 180. P. 1483.
33. *Kondratyuk L. A., Lev F. M.* // Sov. J. Nucl. Phys. 1977. V. 26. P. 153.
34. *Kondratyuk L. A., Lev F. M., Shevchenko L.V.* // Sov. J. Nucl. Phys. 1979. V. 29. P. 558.
35. *Kondratyuk L. A., Lev F. M., Shevchenko L. V.* // Phys. Lett. B. 1981. V. 100. P. 448.
36. *Kaptari L. P., Kämpfer B., Dorkin S. M., Semikh S. S.* // Phys. Rev. C. 1998. V. 57. P. 1097.
37. *Kaptari L. P., Kämpfer B., Dorkin S. M., Semikh S. S.* // Few Body Syst. 1999. V. 27. P. 189.
38. *Ladygina N. B.* // Eur. Phys. J. A. 2016. V. 52. P. 199.
39. *Matveev V. A., Muradyan R. M., Tavkhelidze A. N.* // Lett. Nuovo Cimento. 1973. V. 7. P. 719.
40. *Brodsky S. J., Farrar G. R.* // Phys. Rev. Lett. 1973. V. 31. P. 1153; Phys. Rev. D. 1975. V. 11. P. 1309;
Lepage G. P., Brodsky S. J. // Phys. Rev. D. 1980. V. 22. P. 2157.
41. *Polchinski J., Strassler M. J.* // Phys. Rev. Lett. 2002. V. 88. P. 031601.
42. *Gurchin Yu. V. et al.* // Phys. Part. Nucl. Lett. 2007. V. 4. P. 263.
43. *Froehlich I. et al.* // Eur. Phys. J. A. 2010. V. 45. P. 401.
44. *Albers D. et al.* // Eur. Phys. J. A. 2004. V. 22. P. 125.

Received on May 7, 2019.

Редактор *Е. И. Кравченко*

Подписано в печать 20.06.2019.
Формат 60 × 90/16. Бумага офсетная. Печать офсетная.
Усл. печ. л. 1,18. Уч.-изд. л. 1,52. Тираж 275 экз. Заказ № 59719.

Издательский отдел Объединенного института ядерных исследований
141980, г. Дубна, Московская обл., ул. Жолио-Кюри, 6.
E-mail: publish@jinr.ru
www.jinr.ru/publish/